RSC Advances

PAPER

View Article Online
View Journal | View Issue

Check for updates

Cite this: *RSC Adv.*, 2020, **10**, 15124

Recyclable polyether–polyquaternium grafted SiO_2 microsphere for efficient treatment of ASP flooding-produced water: oil adsorption characteristics and mechanism†

Hao Sun,[ab] Xin He,[c] Qian Tang[ab] and Xiaobing Li *[a]

In this work, an interfacially active PPA@SiO_2 microsphere for ASP flooding-produced water treatment was synthesized by grafting polyether–polyquaternium (PPA) copolymer onto mesoporous hydrated silica (SiO_2). This PPA@SiO_2 microsphere integrates both demulsification and adsorption functionalities. The physicochemical properties of the SiO_2 variants were monitored *via* SEM, BET, XPS, contact angle and zeta potential tests. When disposing of a simulated alkali–surfactant–polymer flooding produced water that contained 500 mg L^{-1} oil, this functional PPA@SiO_2 microsphere exhibited an oil removal efficiency of 78.0% at 1.0 g L^{-1} dosage, which is higher than that of pristine SiO_2 (39.1%) and hydrophobic modified SiO_2 (54.2%). This remarkable oil removal efficiency was attributed to its abilities to destabilize and aggregate the emulsified oil droplets. Oil micromorphology test results indicated that PPA@SiO_2 could aggregate the fine oil droplets into oil clusters, which significantly favors the oil–water separation efficiency. An adsorption kinetics and thermodynamics study manifested that oil adsorption onto PPA@SiO_2 was an exothermic process, mainly dominated by external surface adsorption, which agreed with the BET and micromorphology study. Furthermore, the oil adsorption mechanism has been explored and confirmed according to all the experimental results. This modification protocol significantly reduced the PPA consumption and it was also found that the loaded oil onto PPA@SiO_2 could be effectively separated through a petroleum ether extraction process, so as to recycle the carrier particles. This novel PPA@SiO_2 microsphere with its high oil removal efficiency offers technical promise and huge potential for oily wastewater treatment.

Received 19th January 2020
Accepted 5th April 2020

DOI: 10.1039/d0ra00597e

rsc.li/rsc-advances

Open Access Article. Published on 17 April 2020. Downloaded on 4/29/2026 5:20:50 AM.
This article is licensed under a Creative Commons Attribution-NonCommercial 3.0 Unported Licence.

1 Introduction

Alkali–surfactant–polymer (ASP) flooding is a typical tertiary oil recovery technology, in which alkali, surfactant and polymer are injected as displacement agents. By enhancing oil phase fluidity and water injection viscosity to weaken the adsorption affinity of crude oil on the rock strata, the oil recovery rate has proved to be 20% higher than that of water flooding.[1,2] With the popularization and application of ASP flooding technology, a large amount of ASP flooding produced water has been produced. This wastewater contains a lot of residual oil displacement agents, as well as mineral components, crude oil and microorganisms. Under the high shear condition, the oil displacement surfactants adsorbs on the oil–water interface to form a dense interfacial film, which making the ASP produced water seriously emulsified as a stable oil-in-water (O/W) emulsion.[3–5] If ASP flooding produced water is not treated or fails to meet reinjection standard after treatment, the residual oil substances will damage water injection equipment, block pipeline, pollute water body and destroy ecological balance of oil field.[6] This industrial process has incurred oil pollution in the hydrosphere, lithosphere, biosphere, and anthroposphere, usually at health-endanger levels.[7,8]

Previous researches have pointed out that the destabilization and coalescence of fine oil droplets mainly dominated the ASP flooding produced water treatment efficiency.[9] To achieve the demulsification and oil–water separation, several techniques includes gravity settling, flotation, ultrasonic, membrane, adsorption, biological and chemical treatments have been widely investigated.[10–14] Chemical demulsifiers have proved effective for oil–water separation which can effectively destroy the oil–water interfacial film and promote the

[a]National Engineering Research Center of Coal Preparation and Purification, China University of Mining and Technology, Xuzhou 221116, Jiangsu, China. E-mail: Xiaobing.li@cumt.edu.cn; Tel: +86 13512568890

[b]School of Chemical Engineering and Technology, China University of Mining and Technology, Xuzhou 221116, Jiangsu, China

[c]Key Laboratory of Coalbed Methane Resources and Reservoir Formation Process of Ministry of Education, China University of Mining and Technology, Xuzhou 221008, China

† Electronic supplementary information (ESI) available. See DOI: 10.1039/d0ra00597e

This journal is © The Royal Society of Chemistry 2020

Open Access Article. Published on 17 April 2020. Downloaded on 4/29/2026 5:20:50 AM.
This article is licensed under a Creative Commons Attribution-NonCommercial 3.0 Unported Licence.

coalescence of oil droplets.[15] However, high consumption of chemical demulsifiers may lead to a series of economic and environmental issues.[16,17]

Adsorption was also employed to remove the oil substances from the wastewater and it was considered to be cost-effective.[18] To achieve the fast oil–water separation, the ideal oil adsorbent should exhibit the following characteristics: hydrophobicity and oleophilicity, nontoxic, proper structure, high adsorption capacity and good recyclability.[19,20] Li *et al.* employed surfactant-modified sepiolite to remove emulsified oil from the ASP flooding wastewater. The loading cationic surfactants lead to a charge inversion from negative to positive and they noted that the adsorption of emulsified oil by clay minerals could be greatly improved by replacing the inorganic cations with certain organic cations.[21] Zhou *et al.* synthesized a cetyltrimethyl-ammonium bromide-modified polystyrene resin (R-CTAB) to dispose the O/W emulsion and the R-CTAB was found to more capable to remove emulsified oil than a coal-based activated carbon.[22] They noted that oil droplets in R-CTAB effluent was much easier to coalesce together than that of pristine resin or activated carbon, which was mainly attributed to the ability of R-CTAB to reduce negative potential. This also highlighted the importance of surface potential and interfacial activity in emulsified oil adsorption. In such a scheme, several interfacially active functional oil adsorbents were synthesized based on zeolite, kapok fiber, bentonite, chitosan and Fe_3O_4 carriers.[23–27]

In our previous work, an environmental-friendly polyether–polyquaternium (PPA) demulsifier that integrated both the polyether and polyquaternium functionalities was synthesized to demulsify the O/W emulsion.[28] The PPA achieved higher demulsification efficiency than a commercial demulsifier and the demulsification mechanism of PPA has also been systematically investigated.[28] To further improve the oil–water separation efficiency and reduce PPA consumption, the surface grafting protocol was employed to prepare a PPA@SiO_2 microsphere. This functional PPA@SiO_2 microsphere integrated both the demulsification and adsorption functionalities. Given the demulsification mechanism, the oil adsorption mechanism and the relationship between the structure and adsorption characteristics should be further pursued. To this end, the objectives of this study herein have been to investigate the oil removal characteristics from the perspective of adsorption and explore the oil adsorption mechanism of this novel PPA@SiO_2 microsphere.

2 Experimental

2.1 Material

The crude oil used in this research was directly sampled from the Daqing oilfield (China). A fly ash based hydrated silica ($SiO_2 \cdot nH_2O$) was purchased from the Vanke silicon material technology Co., Ltd. Silicone oil, epoxy ether and methyl ether (Diweilai Technology Co., Ltd. Hangzhou, China) were purchased to prepare the polyether. Polyethylene polyamine, epichlorohydrin, chloroplatinic acid, silane coupling agent (3-methyl propyl trimethoxy silane (MPS)), sodium hydroxide, sodium chloride, sodium bicarbonate, polyacrylamide, sodium dodecyl benzene sulfonate (SDBS) and petroleum ether were obtained from Tianjin Chemical Reagent Factory (Tianjin, China). All these chemicals were AR grade.

2.2 Preparation of PPA@SiO_2 microsphere

Polyether–polyquaternium (PPA, molecular weight: 2684–12 862 Da) was synthesized *via* the epoxide-opening reaction between polyether and polyquaternium as we previously reported.[28] The hydrophobic modification was conducted by reacting hydrated silica with the silane coupling agent.[29] Then, the PPA@SiO_2 microsphere was obtained by grafting PPA onto the hydrophobic silica (MPS–SiO_2) through the hydrosilylation reaction which was catalyzed by chloroplatinic acid (see Fig. 1). For this process, 3.5 g MPS–SiO_2, 7.0 g PPA, 50 μg g^{-1} chloroplatinic acid and 50 mL isopropanol were added into a round-bottomed flask and reacted for 6 h at 70 °C.

2.3 Characterization

Pore volume distributions and surface area of the SiO_2 variants were monitored by an automated specific surface area analyzer (BELSORP-max, MicrotracBEL, JAPAN). Contact angles of the SiO_2 variants were monitored using a Contact Angle Meter (DSA100, Kruss, Germany); and this parameter discerned the solid surface wettability. The micro-topographies of the MPS–SiO_2 and PPA@SiO_2 were obtained by means of a Scanning Electron Microscopy (SEM) (QuantaTM 250, FEI, USA). The surface elemental compositions of the SiO_2 variants were monitored using an X-ray Photoelectron Spectrometer (ESCALAB 250Xi, Thermo Fisher, USA), which employed CASAXPS software to analyze the obtained spectrums.[30] Fourier transform infrared spectroscopy (FTIR) and thermogravimetric (TG) analysis were employed to characterize the surface functional groups and thermal stability of the adsorbent.

For the O/W emulsion, the oil droplets size distribution was determined by a laser particle size analyzer (S3500, Microtrac, USA). The oil droplets morphology before and after adsorption process were observed using an Ultra-Depth Three-Dimensional Microscope (VHX-6000, Keyence, Japan). Additionally, a micro calorimeter (C80, Setaram, France) which equipped with a 3D-sensor was employed to monitor the adsorption heat values of the oil adsorption process. For these tests, 2 mL simulated ASP flooding produced water that contained 1.0 g L^{-1} adsorbent was added into the sample tube and the adsorption values were obtained by integrating the heat flow curves.

2.4 Batch adsorption tests

Batch adsorption tests were conducted to obtain the oil adsorption isotherm data. Initially, 0.05 g adsorbent were added into several bottles that contained 50 mL of simulated ASP flooding produced water with increasing levels C_0 (250–1250 mg L^{-1}) of emulsified oil. The ion composition of the fresh ASP flooding produced water was found to be 53.1 mg L^{-1} $MgCl_2 \cdot 6H_2O$, 6.8 mg L^{-1} Na_2SO_4, 59.7 mg L^{-1} $CaCl_2$, 2442.9 mg L^{-1} $NaHCO_3$ and 1167 mg L^{-1} NaCl; furthermore, the oil displacement agents formula includes 700 mg L^{-1} NaOH, 300 mg L^{-1} SDBS and

Open Access Article. Published on 17 April 2020. Downloaded on 4/29/2026 5:20:50 AM.
This article is licensed under a Creative Commons Attribution-NonCommercial 3.0 Unported Licence.

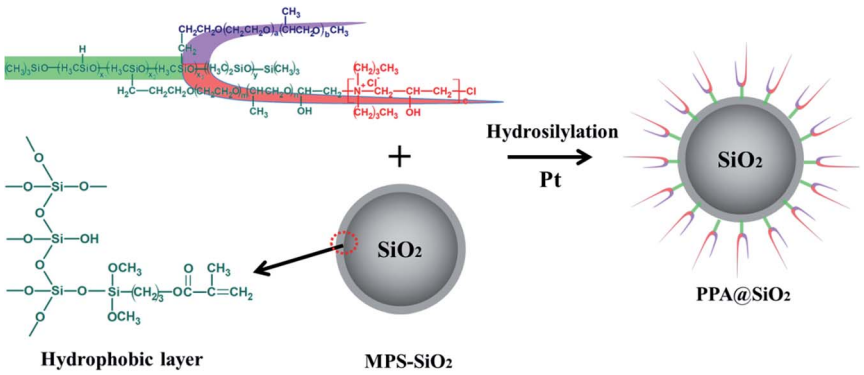

Fig. 1 Preparation of the functional PPA@SiO_2 microsphere.

500 mg L^{-1} PAM. The simulated ASP flooding produced water (with an average oil droplet size of 11.2 μm) was prepared according to the above chemical composition and preparation protocol as we previously reported.[28] These sealed bottles were placed into a water bath and then shaken at selected temperatures to equilibrium. Followed by standing for 30 min, the water phase from the upper layer was taken out, so as to extracted the residual oil using petroleum ether and then measured the equilibrium oil content C_e by an ultraviolet spectrophotometer (UV-4802S, Unico, China). For the kinetics study, the initial oil concentration was 500 mg L^{-1}. Each test was repeated three times, and duplicates varied by less than 3–5%.

2.5 Carrier particles recovery

The petroleum ether extraction protocol was employed to recycle the oil and carrier particles. 0.2 g of oil-loaded PPA@SiO_2 microspheres (which treated simulated produced water with an initial oil level of 500 mg L^{-1}) were wrapped in a filter cartridge and placed into a Soxhlet extractor. The reflux temperature of water bath was controlled to be 83 °C (the petroleum ether boiling range was 60–90 °C), so as to remained the petroleum ether in the micro-boiling state. After extracted by 10 siphon cycles, the residual solids were taken out and dried for further characterizations.

3 Results

3.1 Physicochemical properties of the functional microspheres

Several characterization protocols were employed to investigate the physicochemical properties of the adsorbents. Representative SEM photographs were presented to shown textural structure and approximated size of MPS–SiO_2 and PPA@SiO_2, respectively. Both these two adsorbents were featured by spheroidal and dispersive particles. It was observed that the SiO_2 surface was uniformly coated with silane coupling agent during the hydrophobic modification process (Fig. 2a). The MPS–SiO_2 exhibited a glaze surface and compact structure. Then, during PPA grafting, the outer sphere of PPA@SiO_2 exhibited a sponge-like structure and more interconnected pores appeared during this step which was mainly attributed to the crosslinking of PPA molecules (Fig. 2b). This was consistent with the BET analysis results as shown in Table 1 and the external spongy structure of PPA@SiO_2 was also considered to be more favorable to oil adsorption.[31,32] The pristine SiO_2 particle was characterized as a mesoporous material that about 96% of the total pore volume belongs to mesoporous structure. In the following modification processes, the SiO_2 surface was occupied by the silane coupling agent and PPA molecules which caused the significant reduction in mesopore volume.

To evaluate the lipophilicity or hydrophobicity of these two functional microspheres, the contact angle tests with water and diesel oil were respectively conducted (see Fig. 2c and Table 1). The pristine SiO_2 is a hydrophilic material and its contact angle with water is 2–5 degree. After silane coupling agent loading, the contact angle with water increased to 90.2 degree and the MPS–SiO_2 surface changed to hydrophobic property. Followed by PPA grafting, the hydrophobicity was further enhanced due to the double organic layers onto the SiO_2 surface, which was more favorable to capture the oil droplets.

The thermal stability of these two microspheres was investigated *via* thermogravimetric (TG) analysis as illustrated in Fig. 2d. The agravic peaks before 150 °C were corresponding to the escape of free moisture and gases (such as CO_2) from the pores.[33] In the 150–600 °C range, an obvious mass loss peak appeared at 410 °C and the severe weight loss of MPS–SiO_2 was mainly attributed to the decomposition of the silane coupling agent. For PPA@SiO_2, higher mass loss rate and additional agravic peak at 500–600 °C were exhibited, which were ascribed to the volatilization of weakly-linked PPA and rupture of cross-linked PPA, respectively. The final mass loss rates of MPS–SiO_2 and PPA@SiO_2 was determined to be 37.6% and 42.6%, so it was inferred that the mass fraction of PPA demulsifier onto PPA@SiO_2 was 5%.

The surface elemental composition changes during the modification processes were also monitored by XPS (Table 1). The pristine SiO_2 used in this work was composed of Si and O which exhibited ultrahigh purity. After hydrophobic modification, the C ratio markedly increased to 45.2% which was attributed to the loaded silane coupling agent, and this value further increased to 50.1% because of PPA grafting. Moreover, the appearances of N and Cl on PPA@SiO_2 surface were ascribed

 This journal is © The Royal Society of Chemistry 2020

Open Access Article. Published on 17 April 2020. Downloaded on 4/29/2026 5:20:50 AM.
This article is licensed under a Creative Commons Attribution-NonCommercial 3.0 Unported Licence.

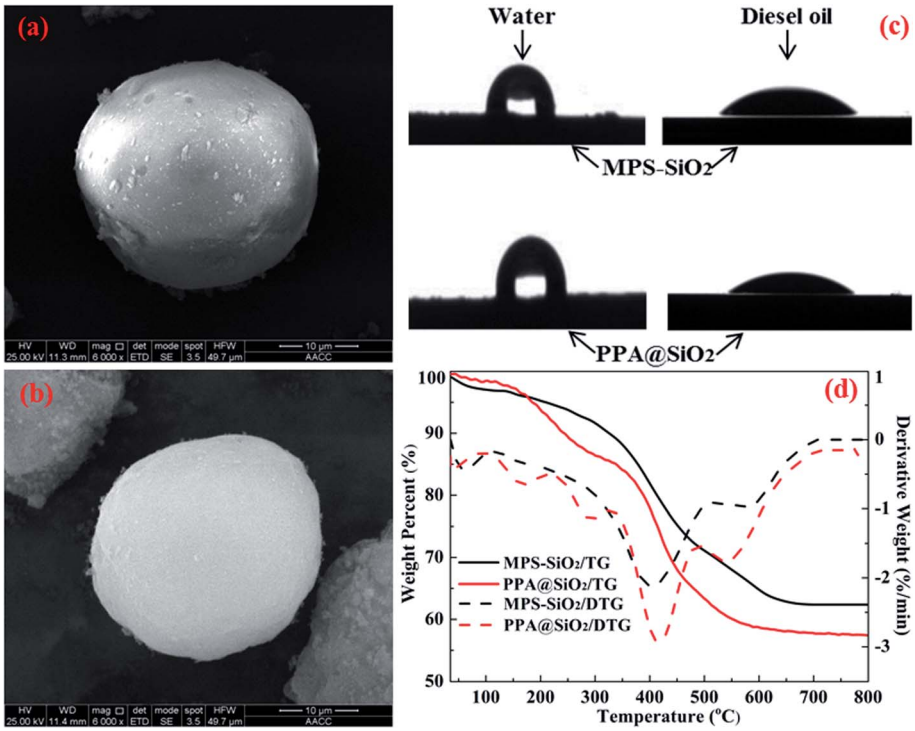

Fig. 2 SEM images of (a) MPS–SiO_2 and (b) PPA@SiO_2; (c) contact angles and (d) TG/DTG curves for the MPS–SiO_2 and PPA@SiO_2 microspheres.

to the polyquaternium branch of PPA. For the surface potential of the SiO_2 variants, the zeta potential of the pristine SiO_2 was determined to be −33.7 mV and increased to −26.5 mV for MPS–SiO_2 which was attributed to the consumption of hydroxyl groups during the hydrophobic modification process. Then, the zeta potential further increased to −13.4 mV due to the positively charged polyquaternium grafting.

3.2 Adsorption kinetics

The kinetics study of oil adsorption was required to investigate the oil diffusion behaviors and determine the optimum operation time, so as to improve the oil removal efficiency. As shown in Fig. S1 (see ESI†), the oil adsorption rate was initially high because more adsorption sites on the adsorbents were available and oil was easily adsorbed on these sites. The adsorption equilibrium was reached within 80 min and it was also found that the PPA@SiO_2 (390.0 mg g^{-1}) microsphere exhibited higher adsorption capacity than MPS–SiO_2 (270.1 mg g^{-1}) and other reported adsorbents.[21,34]

Moreover, there kinetic models: the pseudo-first order and pseudo-second order models were used to further analyze the adsorption kinetic process, which can be described as:[35]

$$\ln(q_e - q_t) = \ln q_e - k_1 t \quad (1)$$

Table 1 Physicochemical parameters of the SiO_2 variants following each modification step

		SiO_2 variants		
Methods	Parameters	SiO_2	MPS–SiO_2	PPA@SiO_2
BET analysis	Surface area (m^2 g^{-1})	186.6	39.2	32.6
	V_{micro}[a] (cm^3 g^{-1})	0.027	0.016	0.019
	V_{meso}[a] (cm^3 g^{-1})	0.745	0.091	0.069
Contact angle (deg.)	With water	2–5	90.2	93.8
	With oil	—	30.4	25.7
Elemental composition (atomic%)	Si2p	29.5	17.5	14.8
	O1s	70.5	37.3	32.0
	C1s	ND[b]	45.2	50.1
	N1s	ND[b]	ND[b]	1.9
	Cl2p	ND[b]	ND[b]	1.2
Surface potential	Zeta potential (mV)	−33.7	−26.5	−13.4

[a] V_{micro} is the cumulative micropore (<20 Å) volume; V_{meso} is the mesopore (20–500 Å) volume. [b] ND means not detected.

Open Access Article. Published on 17 April 2020. Downloaded on 4/29/2026 5:20:50 AM.
This article is licensed under a Creative Commons Attribution-NonCommercial 3.0 Unported Licence.

$$\frac{t}{q_t} = \frac{1}{k_2 q_e^2} + \frac{t}{q_e} \quad (2)$$

where q_t and q_e (mg g^{-1}) are the oil adsorption capacity at time t (min) and equilibrium state; k_1 (min^{-1}) and k_2 (g (mg^{-1} min^{-1})) represent the adsorption rate constant of pseudo-first order and pseudo-second order model, respectively.

The pseudo-second order modeling of these experimental results yielded a correlation coefficient R^2 of >0.99, which represented the best fit of the kinetics data. The calculated q_{e2} was also closer to the experimental $q_{e,exp}$ value (Table 2). This indicates the validity of the pseudo-second order kinetic model for emulsified oil adsorption systems which is not wondering as this model was frequently used to describe oil or other organics adsorption kinetics onto other adsorbents.[35,36] Furthermore, the fast adsorption equilibrium manifested that the emulsified oil adsorption rate onto the microspheres was primarily determined by the surface or external diffusion rather than pore diffusion process. However, the pristine SiO_2 achieved an oil adsorption capacity of 195.8 mg g^{-1} within 480 min, this relatively longer equilibrium time emphasizes the pore diffusion behaviors of oil adsorption onto SiO_2. This phenomenon was also consistent with the BET results.

3.3 Adsorption thermodynamics

The effect of adsorbents dosage on adsorption capacity was investigated as shown (see Fig. S2 in ESI†). It was observed that the more the adsorbents dosage, the lower the oil adsorption capacity and the higher oil removal efficiency were. At the PPA@SiO_2 dosage of 3.0 g L^{-1}, over 95% of emulsified oil was removed when the initial oil concentration was 500 mg L^{-1}; and the treated water exhibited a high clarity. The oil removal efficiency was 78.0% at the dosage of 1.0 g L^{-1}, this corresponding to a 50 mg L^{-1} PPA dosage which was calculated by the 5% PPA loading in the TG/TGA analysis. During the demulsification process of PPA, the destabilized oil droplets conglomerated into large oil droplets and then floated up to the liquid surface. However, after demulsification by PPA@SiO_2, the coalesced oil droplets sink to the bottom of the liquid along with the SiO_2 cores. It should be noted that the larger the size of oil droplets, the higher the oil–water separation efficiency. The average size of aggregated oil droplets was determined to be 441 μm at 1.0 g L^{-1} PPA@SiO_2 dosage, which was much higher than that (221 μm) at 50 mg L^{-1} PPA dosage (see Fig. S3 in ESI†). As we previously reported, about 100 mg L^{-1} of PPA was added to achieve the same oil removal efficiency of 78.0%.[28] This result highlighted the integrated demulsification and adsorption functionalities of PPA@SiO_2.

Langmuir and Freundlich isotherms tests were conducted at 298, 308 and 318 K, so as to evaluate the oil adsorption capacities (Fig. S4 in ESI†). In all cases, the isotherms fit quite well (R^2 > 0.99, Table 2) to the Freundlich equation which can be described as:[37,38]

$$\ln q_e = \ln k_F + 1/n \ln C_e \quad (3)$$

where k_F (mg g^{-1} (L mg^{-1})$^{-1/n}$) and n are the Freundlich model constants; C_e represents the equilibrium oil concentration. This indicates that the oil uptake onto microspheres exhibited nonhomogeneous and multilayer adsorption. It was also noted that monolayer adsorption could occur at low oil concentration, which was mainly attributed to the active site occupation by the single oil droplet. Then, the emulsified oil droplet could be demulsified by the PPA branches and then aggregated onto the PPA@SiO_2 surface to form multilayer oil. This adsorption mechanism was completely different from the ionic contaminants we have reported before;[37] and it was inferred that oil adsorption was governed by hydrophobic interaction.

Table 2 also listed the adsorption heat values of the oil adsorption process at various temperatures. The negative

Table 2 Oil adsorption kinetics and isotherm models parameters onto MPS–SiO_2 and PPA@SiO_2 microspheres

		SiO_2 variants					
Models	Parameters	MPS–SiO_2			PPA@SiO_2		
Kinetics models							
Experimental	$q_{e,exp}$/(mg g^{-1})	270.1			390.0		
Pseudo-first order	q_{e1}/(mg g^{-1})	174.8			279.9		
	k_1/(min^{-1})	0.068			0.083		
	R_1^2	0.973			0.968		
Pseudo-second order	q_{e2}/(mg g^{-1})	286.5			401.6		
	k_2/(g (mg^{-1} min^{-1}))	6.1×10^{-4}			6.8×10^{-4}		
	R_2^2	0.998			0.999		
Isotherm model							
Freundlich model	Temperature (K)	298	308	318	298	308	318
	k_F (mg g^{-1} (L mg^{-1})$^{-1/n}$)	1.85	1.15	1.08	60.3	18.2	6.1
	$1/n$	0.93	0.97	1.01	0.43	0.60	0.77
	R^2	0.991	0.998	0.996	0.991	0.995	0.997
	Adsorption heat[a] (J g^{-1})	−5.9	−2.6	−1.7	−20.9	−11.7	−5.3

[a] The adsorption heat was monitored at the initial oil concentration of 500 mg L^{-1}.

 This journal is © The Royal Society of Chemistry 2020

Open Access Article. Published on 17 April 2020. Downloaded on 4/29/2026 5:20:50 AM.
This article is licensed under a Creative Commons Attribution-NonCommercial 3.0 Unported Licence.

adsorption heat values demonstrated the exothermic nature of oil adsorption onto these two functional microspheres, which was supported by the decreasing oil adsorption capacity with the increase of temperature. The PPA@SiO_2 exhibited a stronger adsorption effect than MPS–SiO_2, which agreed with the principle of the oil adsorption capacity. This could be interpreted that the oil adsorption heat of MPS–SiO_2 was mainly attributed to the hydrophobic interaction. However, the oil adsorption onto PPA@SiO_2 also included the electrostatic neutralization and attraction, which further enhanced the thermal effect.

3.4 Oil droplets micromorphology

Fig. 3 exhibited the micromorphology of the oil droplets in the simulated ASP flooding produced water, PPA@SiO_2 treated water and oil-loaded PPA@SiO_2 microspheres. It was observed that the oil substances exist in the ASP flooding produced water as various micron-sized oil droplets (Fig. 3a). Some ultrafine oil droplets were also stably distributed and the average oil droplets size was determined to be 11.2 μm. After the 1.0 g L^{-1} PPA@SiO_2 treatment, most of the large oil droplets were removed and the residual oil is mainly fine (<5.0 μm) oil droplets (Fig. 3b). The residual oil droplets remained in the oil-in-water form and a clear hydration film was observed around the oil droplets. This indicates that large oil droplets were easier to be demulsified and captured than fine species by PPA@SiO_2 microsphere. When more PPA@SiO_2 microspheres were added, abundant PPA onto the microsphere surface were available to further destabilize the residual oil droplets. It was also inferred that PPA@SiO_2 was more favorable to remove fine oil droplets than MPS–SiO_2 at the same dosage. This was consistent with the results as shown in Fig. S2.†

After being adsorbed, the oil droplets sink to the bottle bottom along with the PPA@SiO_2 microspheres as shown in Fig. 3c. This complex sediment was characterized as amorphous clusters with various size (>50 μm) which include the PPA@SiO_2 core and its surrounding aggregated oil. By scanning the oil loaded PPA@SiO_2 *via* XPS (see Fig. S5 in the ESI†), 1.21% of S2p was monitored which was mainly attributed to the adsorbed SDBS molecules onto the microsphere surface and aggregated oil clusters.

3.5 Carrier particles recovery

Fig. 4 shows the FTIR spectra of the SiO_2 variants. All spectra have a hydroxyl groups (–OH) and water molecules peak at the wavelength of 3400 cm^{-1}. The peak at 2960 cm^{-1} and 2850 cm^{-1} were assigned to the stretching vibration of methyl (–CH_3) and methylene (–CH_2–) groups on microspheres surfaces. The peak between 2600–2800 corresponds to the secondary or tertiary amine that was generated by some side reaction during the PPA synthesis process. Peaks at 2165 cm^{-1} and 1480 cm^{-1} were due to the adsorption bands of quaternium (N^+-CH_3) and methylamine (N-CH_3). The stretching bending at 1720 cm^{-1} and 1640 cm^{-1} corresponded to the unsaturated carbonyl group (–C═O) and double carbon bond (–C═C–) that originated from the silane coupling agent. The peaks at wavelength of 1100 cm^{-1} and 470 cm^{-1} were respectively attributed to the stretching and bending vibration of Si–O–Si. After oil loading, these –CH_3 and –CH_2– peaks were strengthened due to the alkyl structure of the adsorbed oil substance. In addition, the disappearance of N^+-CH_3 band also proved the negatively charged oil droplets and SDBS had been adsorbed. After the extraction process, the –CH_3 and –CH_2– peaks strength significantly weakened because of oil desorption. It was noted that

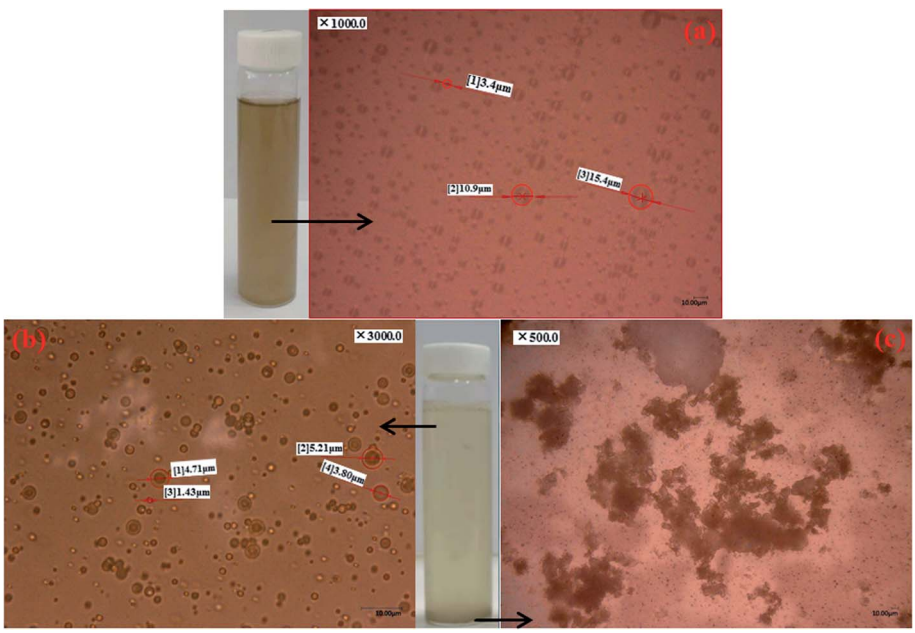

Fig. 3 Micro morphologies of oil droplets in (a) simulated ASP flooding produced water; (b) 1.0 g L^{-1} PPA@SiO_2 treated produced water and (c) oil-loaded PPA@SiO_2 microspheres.

Open Access Article. Published on 17 April 2020. Downloaded on 4/29/2026 5:20:50 AM.
This article is licensed under a Creative Commons Attribution-NonCommercial 3.0 Unported Licence.

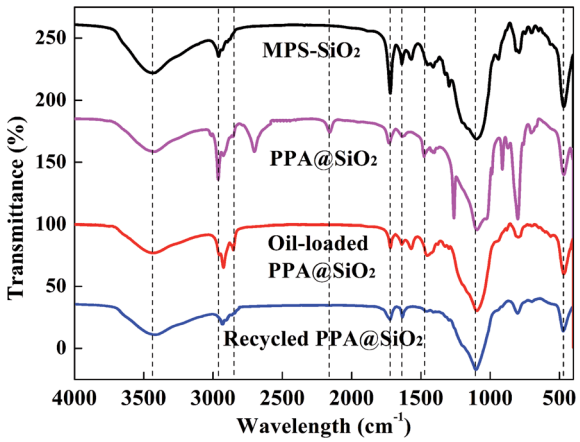

Fig. 4 FTIR spectra of the SiO_2 variants.

the eluotropic oil in the petroleum ether could be recovered by a normal fractional distillation process.[39]

In addition, the surface elemental composition of the recovered carrier particles was monitored *via* XPS. It was found that the recovered carrier particles surface were composed by 40.2% of C1s, 40.2% of O1s, 18.5% of Si2p, 0.6% of N1s and 0.5% of Cl2p (see Fig. S5 in the ESI†). The significant reduction on N1s and Cl2p indicated the elimination or destruction of PPA branch during the extraction procedure. However, this composition was found to be more similar to the data information of MPS–SiO_2 (see Table 1). By combining the FTIR and XPS results, it was inferred that the recycled carrier particles approximately exhibited an intact intermediate (MPS–SiO_2) structure and it could be re-used for PPA grafting.

4 Discussion

The above results support that the PPA@SiO_2 microsphere which integrated the demulsification and adsorption functionalities was more efficient than PPA to dispose the O/W emulsions. By compiling the characterization, micromorphology, adsorption kinetics and thermodynamics data, the oil adsorption mechanism of PPA@SiO_2 was further proposed as illustrated in Fig. 5.

When PPA@SiO_2 microspheres were added into the ASP flooding produced water, the emulsified oil droplets were firstly destabilized by PPA on the surface. The negatively charged oil droplets primarily moved toward to the positively charged PPA@SiO_2 surface *via* the electrostatic force and the compact SDBS network was disrupted by the dart-shaped quaternium branch. Then, the interfacially active polyether branch displaced the SDBS molecules *via* a multipoint adsorption onto oil droplet and achieved the original interfacial film rupture. This significantly reduced the repulsion force between oil droplets and promoted their coalescence.[28]

Following by demulsification, the demulsified oil could be easily captured by the PPA@SiO_2 microsphere and the three oil-loading species were described. First, the demulsified oil droplet could be adsorbed onto the external polyether branch and start to coalesced (Fig. 5a). Second, the demulsified oil droplets diffused into the MPS layer and adsorbed by the hydrophobic force (Fig. 5b). This process was considered to be contributed least to the oil adsorption capacity, which was proved by the weak intra-particle diffusion effect during the adsorption kinetics study. Thirdly, the demulsified small oil droplets aggregated to big oil clusters on the external surface of PPA@SiO_2 microspheres and then attracted other microspheres (Fig. 5c). It should be noted that the PPA@SiO_2 microspheres were well dispersed in aqueous solutions, so the cluster was act as a bridge agent to connect the

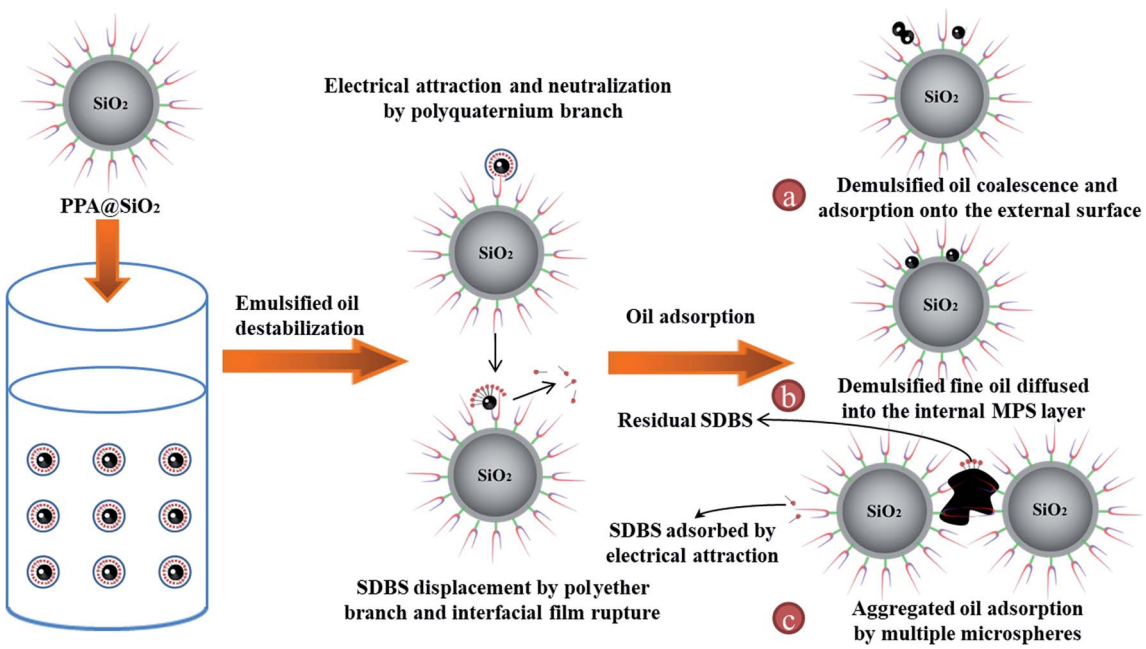

Fig. 5 Schematic diagram of proposed oil adsorption mechanism of PPA@SiO_2 towards the O/W emulsion (a) oil coalescence, (b) oil diffusion, and (c) oil-loaded microspheres aggregation.

 This journal is © The Royal Society of Chemistry 2020

Open Access Article. Published on 17 April 2020. Downloaded on 4/29/2026 5:20:50 AM.
This article is licensed under a Creative Commons Attribution-NonCommercial 3.0 Unported Licence.

PPA@SiO_2 microspheres. We also inferred that this process mainly dominate the adsorption performance.

5 Conclusions

An interfacially active PPA@SiO_2 microsphere has been prepared to dispose the O/W emulsion that originated from the ASP flooding produced water. This novel microsphere integrated the demulsification and adsorption functionalities which exhibited an oil adsorption capacity of 390.0 mg g^{-1} within 80 min at the initial oil concentration of 500 mg L^{-1}; and this is much higher than that of SiO_2 (195.8 mg g^{-1}). The PPA@SiO_2 microspheres primarily destabilized the emulsified oil droplets *via* the electrical neutralization and SDBS displacement effects. Afterwards, the microsphere with excellent hydrophobicity captured the demulsified oil droplets and then aggregated the oil into big oil clusters. Finally, the oil and carrier particles could be efficiently separated *via* a chemical extraction protocol. These unique oil adsorption and recovery properties of PPA@SiO_2 microsphere make it an acceptable alternative oil adsorbent towards the alkaline–surfactant–polymer flooding O/W emulsions.

Conflicts of interest

There are no conflicts to declare.

Acknowledgements

This work was supported by the National Natural Science Foundation of China (No. 51674261).

References

1 F. Chen, H. Jiang, X. Bai and W. Zhang, *J. Ind. Eng. Chem.*, 2013, **19**, 450–457.
2 S. Deng, R. Bai, J. P. Chen, G. Yu, Z. Jiang and F. Zhou, *Colloids Surf., A*, 2002, **211**, 275–284.
3 M. Liu, J. Li and Z. Guo, *J. Colloid Interface Sci.*, 2016, **467**, 261–270.
4 A. M. A. Pintor, V. J. Vilar, C. M. Botelho and R. A. Boaventura, *Chem. Eng. J.*, 2016, **297**, 229–255.
5 F. Zhang, J. Ouyang, Y. He, D. Wang and X. Feng, *Chem. Technol. Fuels Oils*, 2012, **47**, 434–439.
6 A. Fakhru'l-Razi, A. Pendashteh, L. C. Abdullah, D. R. A. Biak, S. S. Madaeni and Z. Z. Abidin, *J. Hazard. Mater.*, 2009, **170**, 530–551.
7 C. Lyu, D. He, Y. M. Chang, Q. H. Zhang, F. Wen and X. S. Wang, *Sci. Total Environ.*, 2019, **688**, 1124–1136.
8 S. Jiménez, M. Andreozzi, M. M. Micó, M. G. Álvarez and S. Contreras, *Sci. Total Environ.*, 2019, **666**, 12–21.
9 X. B. Li, H. X. Xu, J. T. Liu, J. Zhang, J. Li and Z. L. Gui, *Sep. Purif. Technol.*, 2016, **165**, 101–106.
10 A. Alabresm, Y. P. Chen, A. W. Decho and J. Lead, *Sci. Total Environ.*, 2018, **630**, 1292–1297.
11 S. Fang, T. Chen, B. Chen, Y. Xiong, Y. Zhu and M. Duan, *Colloids Surf., A*, 2016, **511**, 47–54.
12 H. G. Nasiri, R. Kadkhodaee and M. T. H. Mousavian, *Sep. Sci. Technol.*, 2012, **47**, 1985–1990.
13 M. R. A. Radzuan, M. A. A. Belope and R. B. Thorpe, *Chem. Eng. Res. Des.*, 2016, **115**, 19–33.
14 R. S. Souza, P. S. S. Porto, A. M. A. Pintor, G. Ruphuy and J. P. V. Vítor, *Chem. Eng. J.*, 2015, **285**, 709–717.
15 M. Duan, J. He, D. J. Li, X. J. Wang, B. Jing, Y. Xiong and S. W. Fang, *J. Pet. Sci. Eng.*, 2019, **175**, 317–323.
16 S. Sakthivel, R. L. Gardas and J. S. Sangwai, *Energy Fuels*, 2016, **30**, 2514–2523.
17 J. Wang, F. L. Hu, C. Q. Li, J. Li and Y. Yang, *Sep. Purif. Technol.*, 2010, **73**, 349–354.
18 J. Wang, Y. Zheng and A. Wang, *Mar. Pollut. Bull.*, 2013, **69**, 91–96.
19 Y. Zeng, C. Yang, J. Zhang and W. Pu, *J. Hazard. Mater.*, 2007, **147**, 991–996.
20 M. O. Adebajo, R. L. Frost, J. T. Kloprogge, O. Carmody and S. Kokot, *J. Porous Mater.*, 2003, **10**, 159–170.
21 Y. F. Li, M. X. Wang, D. J. Sun, Y. J. Li and T. Wu, *Appl. Clay Sci.*, 2018, **157**, 227–236.
22 Y. B. Zhou, X. Y. Tang, X. M. Hu, S. Fritschi and J. Lu, *Sep. Purif. Technol.*, 2008, **63**, 400–406.
23 M. Al-Yaari, I. A. Hussein and A. Al-Sarkhi, *Appl. Clay Sci.*, 2014, **95**, 303–309.
24 T. T. Lim and X. Huang, *Chemosphere*, 2007, **66**, 955–963.
25 H. H. Mao, F. Cheng, C. Lei, Z. Y. Feng, Q. Q. Wang, B. L. Chu, Y. Kong, Y. X. Tao, C. Yao and S. X. Zuo, *Ind. Eng. Chem. Res.*, 2019, **58**, 18613–18622.
26 J. Yang, H. Song, X. Yan, H. Tang and C. Li, *Cellulose*, 2014, **21**, 1851–1857.
27 K. Y. A. Lin, Y. C. Chen and S. Phattarapattamawong, *J. Colloid Interface Sci.*, 2016, **478**, 97–106.
28 H. Sun, Q. Q. Wang, X. B. Li and X. He, *Fuel*, 2020, **263**, 116770.
29 F. An, B. Gao and X. Feng, *Chem. Eng. J.*, 2009, **153**, 108–113.
30 X. He, H. Sun, B. Zhao, X. W. Chen, X. X. Zhang and S. Komarneni, *Fuel*, 2018, **233**, 759–768.
31 R. R. Li, J. Y. Ren, Y. P. Xu, G. L. Zhang, D. F. Wang, Z. Y. Wu and D. Q. Cai, *Sci. Total Environ.*, 2019, **688**, 1124–1136.
32 J. Ma, W. H. Zhu, P. O. Lartey and W. Qin, *J. Nanosci. Nanotechnol.*, 2020, **20**, 1540–1553.
33 F. Li, X. C. Liu, L. Song, X. H. Wang, Y. Zhang, T. W. Cui and H. Y. Tang, *Powder Technol.*, 2013, **247**, 19–23.
34 T. H. Ibrahim, M. A. Sabri and M. I. Khamis, *Environ. Technol.*, 2019, **40**, 3337–3350.
35 A. L. A. Abirami, P. S. Kumar, D. G. Prakash, A. Ravirajan, A. Umasankaran, P. Narayanan, K. Ravishankar, C. S. Kumar, S. Nagaraju and K. P. J. Reddy, *Sep. Purif. Technol.*, 2020, **234**, 116095.
36 S. L. Hailu, B. U. Nair, M. Redi-Abshiro, I. Diaz and M. Tessema, *J. Environ. Chem. Eng.*, 2017, **5**, 3319–3329.
37 H. Sun, F. S. Cannon and X. He, *Sci. Total Environ.*, 2019, **660**, 577–585.
38 S. M. Davoodi, M. Taheran, S. K. Brar, R. Galvez-Cloutier and R. Martel, *Fuel*, 2019, **251**, 57–72.
39 H. S. Hu, Y. L. Wu and M. D. Yang, *Biomass Bioenergy*, 2018, **108**, 487–500.